



Article

A TiO₂ Coated Carbon Aerogel Derived from Bamboo Pulp Fibers for Enhanced Visible Light Photo-Catalytic Degradation of Methylene Blue

Jian Zhang¹, Wei Yuan¹, Tian Xia¹, Chenghong Ao¹, Jiangqi Zhao¹, Bingxue Huang¹, Qunhao Wang¹, Wei Zhang^{1,2,*}  and Canhui Lu^{1,2,*}

- ¹ State Key Laboratory of Polymer Materials Engineering, Polymer Research Institute at Sichuan University, Chengdu 610065, China; pirl03721@126.com (J.Z.); Union_sing@126.com (W.Y.); xiatian0621scu@163.com (T.X.); chenghongaocd@163.com (C.A.); scu_jqz@163.com (J.Z.); hbx15756376063@126.com (B.H.); 17839918692@163.com (Q.W.)
- ² Advanced Polymer Materials Research Center of Sichuan University, Shishi 362700, China
- * Correspondence: weizhang@scu.edu.cn (W.Z.); canhuilu@scu.edu.cn (C.L.); Tel.: +86-28-85460607 (W.Z.); Fax: +86-28-85402465 (W.Z.)

Abstract: Carbon aerogels (CA) derived from bamboo cellulose fibers were coupled with TiO₂ to form CA/TiO₂ hybrids, which exhibited extraordinary performance on the photo-catalytic degradation of methylene blue (MB). The structure and morphology of CA/TiO₂ were characterized by field emission scanning electron microscopy, Fourier transform infrared spectroscopy, X-ray photoelectron spectroscopy, X-ray diffraction, and Raman spectrum. The CA displayed a highly porous and interconnected three-dimensional framework structure, while introducing the catalytic active sites of TiO₂ onto the aerogel scaffold could remarkably enhance its photo-catalytic activity. The adsorption and photo-catalytic degradation of MB by the CA/TiO₂ hybrid were investigated. The maximum adsorption capacity of CA/TiO₂ for MB was 18.5 mg/g, which outperformed many similar materials reported in the literature. In addition, compared with other photo-catalysts, the present CA/TiO₂ demonstrated superior photo-catalytic performance. Almost 85% of MB in 50 mL solution with a MB concentration of 10 mg/L could be effectively degraded by 15 mg CA/TiO₂ in 300 min.

Keywords: cellulose; carbon aerogel; titanium dioxide; photo-catalytic degradation; methylene blue



Citation: Zhang, J.; Yuan, W.; Xia, T.; Ao, C.; Zhao, J.; Huang, B.; Wang, Q.; Zhang, W.; Lu, C. A TiO₂ Coated Carbon Aerogel Derived from Bamboo Pulp Fibers for Enhanced Visible Light Photo-Catalytic Degradation of Methylene Blue. *Nanomaterials* **2021**, *11*, 239. <https://doi.org/10.3390/nano11010239>

Received: 27 December 2020
Accepted: 5 January 2021
Published: 18 January 2021

Publisher's Note: MDPI stays neutral with regard to jurisdictional claims in published maps and institutional affiliations.



Copyright: © 2021 by the authors. Licensee MDPI, Basel, Switzerland. This article is an open access article distributed under the terms and conditions of the Creative Commons Attribution (CC BY) license (<https://creativecommons.org/licenses/by/4.0/>).

1. Introduction

The vast application of dyes in the light industry, especially in textile, leather, paper, plastics, and so on, to obtain colorful products has become a recurring phenomenon. However, residue dyes in effluents raise huge environmental problems which threaten ecosystems, including those on which we as human beings rely. For example, as one of the most frequently used dyes, the discharge of methylene blue (MB) is a major concern due to its adverse impacts on health [1]. Inhaling MB can cause accelerated or difficult breathing. If orally administrated, the affected person may show some strong clinical responses such as burning sensations, mental confusion, vomiting, nausea, and methemoglobinemia [2–4]. Hence, the development of eco-friendly and more efficient strategies for the removal of MB in wastewater is of great significance for the aquatic environment.

So far, various methods have been applied to tackle MB pollution in wastewater, such as sonochemical degradation [5], cation exchange [6], electrochemical degradation [7], micellar-enhanced ultrafiltration [8], Fenton-biological treatment [9], and adsorption/precipitation [10]. Among them, photo-catalysis shows promise to settle this problem. As is well known, photo-catalysis can fully degrade organic dyes into small molecules without any secondary pollution and is free from the subsequent separation process [11–13]. Titanium dioxide (TiO₂) is one of the most popular photo-catalysts, owing to its excellent photo-catalytic performance, low cost, superior stability, and non-toxicity.

Meanwhile, doping with nonmetals (C, N, S) has been proven to be able to produce photo-catalysts with higher efficiencies under visible light [14–19]. Specifically, its combination with carbon materials can largely improve the visible light response and photo-catalytic activity [20–34]. For example, Esther et al. prepared a carbon xerogel–TiO₂ composite through a sol–gel process followed by pyrolysis using resorcinol and formaldehyde as the carbon sources [35]. The micro-morphology analysis indicated that the carbon sphere was coated by TiO₂. The interaction between carbon and TiO₂, as well as the oxygen vacancies caused by carbonization, could narrow the band gap of TiO₂ and consequently improve the visible light response of the composite.

Nonetheless, most photo-catalysts reported previously showed lots of defects and boundaries caused by the aggregation of the carbon matrix. This will inevitably result in the recombination of photo-generated electrons and holes and decrease the photo-catalytic efficiency. Carbon aerogels, a novel species of porous carbon material, have shown promise in various fields [36]. Nonetheless, carbon aerogels are usually derived from synthetic organic compounds. This not only causes fast consumption of the limited non-renewable resources but also brings about secondary pollution to the environment after their service life. Moreover, there are only limited studies focusing on the application of carbon aerogels in photo-catalysis.

Herein, we present a carbon/TiO₂ hybrid aerogel (CA/TiO₂) using bamboo pulp fibers as the carbon source for the photo-catalytic degradation of MB under visible light. Bamboo is an abundant natural resource in Southwest China. Compared with wood, it only takes several months to grow. In addition, it has a high content of cellulose, with many distinguishing features such as high strength, high flexibility, and low density. Additionally, our previous study suggested that bamboo pulp fibers could be used as a promising precursor material for the preparation of carbon aerogels with ultra-lightweight and high porosity features [37]. Meanwhile, TiO₂ was hydrothermally anchored on the surface of fibers and distributed homogeneously along the fibers. The obtained hybrid aerogel was still highly porous with an interconnected three-dimensional framework. This structure could effectively suppress the generation of boundaries and defects and hence decrease the probability of recombination between photo-generated electrons and holes, leading to improved photo-catalytic activity under visible light. In the meantime, the aerogel structure also favored the adsorption of MB as it promoted dye diffusion and provided a higher specific surface area.

2. Materials and Methods

2.1. Materials

The bamboo pulp with a solid content of 25 wt% was supplied by Yongfeng Paper Co., Ltd., Muchuan, China. Tetrabutyl titanate (Ti(OBu)₄), acetic acid, and ethanol were of analytical grade and supplied by Kelong Chemical Reagent Co., Ltd., Chengdu, China.

2.2. Synthesis of CA/TiO₂

The CA/TiO₂ was fabricated by a hydrothermal method using bamboo cellulose and Ti(OBu)₄ as the carbon source and titanium dioxide precursor, respectively. In a typical process, bamboo pulp with a determined mass was dispersed in 25 mL deionized water under magnetic stirring to form a homogeneous suspension with a concentration of 1 wt% (solution A). Meanwhile, 1 mL Ti(OBu)₄ was added to 5 mL ethanol containing 2.5 mL acetic acid under stirring to form a light yellow solution (solution B). Next, solution B was added into solution A and stirred for 2 h. The mixture was then transferred into a Teflon-lined stainless-steel autoclave and kept at 150 °C for 6 h. After that, the precipitation was centrifuged while it cooled down to room temperature. The obtained powder was re-dispersed into deionized water. Then, the suspension was freeze-dried at −40 °C for 48 h to obtain the cellulose/TiO₂ hybrid aerogel.

In order to produce CA/TiO₂, the cellulose/TiO₂ hybrid aerogel was subjected to high-temperature carbonization in a tube furnace (OTF1200X, Kejing Materials Technology

Co., Ltd., Shenzhen, China). The sample was heated to 240 °C at a heating rate of 2 °C/min and kept at this temperature for 1 h. Then, the temperature was increased to 400 °C at a rate of 2 °C/min and kept for 1 h. After that, the temperature was raised to 600 °C at 5 °C/min, followed by an isothermal process for 1 h, and then further heated up to 800 °C at a rate of 5 °C/min and kept for another 2 h. Finally, the sample was cooled down to the ambient temperature naturally. All the pyrolysis processes were conducted in a nitrogen atmosphere. For comparison, a pure carbon aerogel was also prepared in a similar way and denoted as CA.

2.3. Characterization

The micromorphology of CA/TiO₂ was observed through field emission scanning electron microscopy (FE-SEM, JEOL JSM-7500F, Tokyo, Japan). The relative contents of the elements were analyzed via energy dispersive X-ray spectroscopy (EDX). Fourier transform infrared spectroscopy (FTIR) and X-ray photoelectron spectroscopy (XPS) were used to characterize the chemical composition of CA/TiO₂. FTIR spectra were acquired from 400 to 4000 cm⁻¹ at a resolution of 4 cm⁻¹ using a FTIR spectrometer (NICOLET 6700, Thermo Fisher Scientific, Waltham, Massachusetts, USA). XPS spectra were recorded on a XPS spectrometer (ESCALAB 250Xi, Thermo Scientific, Waltham, Massachusetts, USA) with an Al K α X-ray source (1486.8 eV). The crystalline structures were observed through X-ray diffraction (XRD, D8 Advance, Bruker, Karlsruhe, German) using Cu K α radiation at a wavelength (λ) of 1.541 Å with 2 θ angle from 10 to 70°. Raman spectra were obtained on a Raman microspectrometer (STA 6000, Perkin Elmer, Waltham, Massachusetts, USA) with an excitation wavelength of 532 nm. Optical absorption behavior was characterized by a double-beam UV–vis spectrophotometer (UV-3600, Mapada Instruments Co., Shanghai, China) equipped with a Praying Mantis diffuse reflectance accessory (DRS); BaSO₄ was used as a reference.

2.4. The Adsorption Performance for MB

A certain amount of CA/TiO₂ was immersed into 20 mL solution with the MB concentration varying from 1 to 20 mg/L under dark conditions and shaken for 2 days at ambient temperature. The residual concentration of MB in the solution was calculated by the absorbance of the measured solution according to the standard curve of the MB. When the adsorption equilibrium was reached, the concentration of the remaining MB was evaluated. The concentration of the MB was detected by a UV–vis spectrophotometer at 664 nm. The adsorption capacity of CA/TiO₂ for MB was calculated by Equation (1):

$$q_e = \frac{V(c_0 - c_e)}{m} \quad (1)$$

where q_e (mg/g) is the adsorption capacity for MB, C_0 and C_e (mg/L) are the concentrations of MB before and after adsorption, respectively, m (g) is the mass of CA/TiO₂, and V (L) is the volume of MB solution.

2.5. Photo-Catalytic Activity Test

The photo-catalytic activity of CA/TiO₂ was monitored via the change of MB concentration under the illumination of an ordinary incandescent lamp (200 W, Shuangyi Lighting Electric Appliance Co., Ltd., Shenzhen, China). Firstly, 15 mg CA/TiO₂ was added into 50 mL MB solution with a concentration of 10 mg/L for MB adsorption under dark conditions. When the adsorption–desorption process reached equilibrium, the mixture was transferred to the irradiation region of visible light. Equal aliquots of solution were withdrawn from the system every 30 min and measured at 664 nm by a UV–vis spectrophotometer to estimate the concentration of the remaining MB. The photo-catalytic performance was evaluated by the ratio of C/C_0 , where C is the initial concentration of MB and C_0 is the concentration of MB at time t . The experiment was conducted for three

times and the average values were presented. In addition, the experimental data of photo-catalytic degradation of MB were fitted to the first-order kinetics model of Equation (2).

$$-\ln \frac{C_t}{C_0} = kt \quad (2)$$

where C_0 , C_t , and k are the initial concentration of MB, the MB concentration at time t , and the rate constant, respectively.

3. Results and Discussion

3.1. Characterization of Materials

Figure 1 shows the morphologies of CA/TiO₂ and CA under different magnifications. Some significant differences can be observed. Compared with CA, the fibers in CA/TiO₂ exhibited a rougher surface, and their average diameter increased from 7.05 to 8.9 μm. As expected, CA/TiO₂ greatly retained the highly porous structure of CA. Figure 1e clearly displays the abundant pores in CA/TiO₂. These pores could not only contribute to the adsorption of MB and strengthen the contact between MB and active sites, but also suppress the formation of boundaries and defects from carbon aggregation. Interestingly, the CA/TiO₂ had a rather low density (18.5 mg/cm³), which was comparable to and even lower than those of some early reported carbon aerogels derived from biomass [38,39]. Additionally, the EDX results (Figure 1g) indicated that the three elements (C, O, and Ti) existed in the aerogel. Along with the SEM image in Figure 1f, it could be confirmed that TiO₂ had been anchored on the carbon fiber scaffold to form a thin layer.

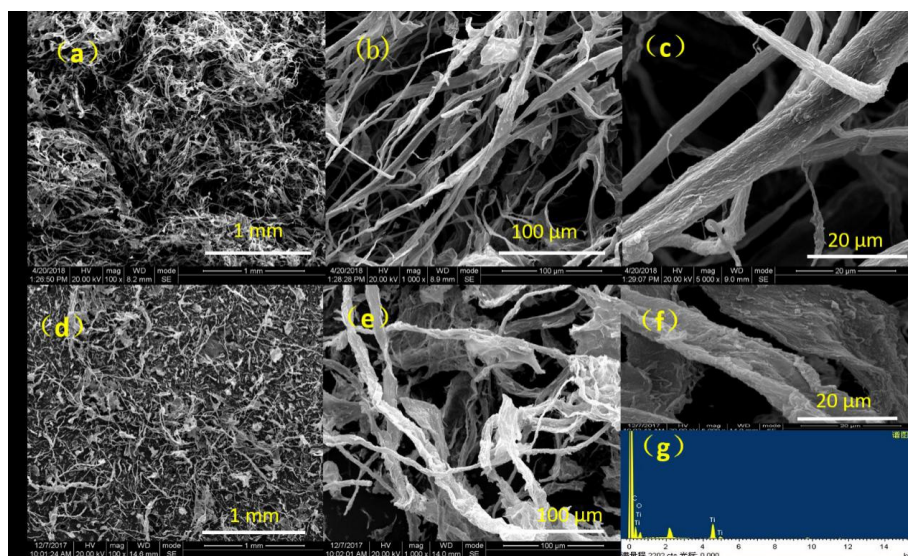


Figure 1. SEM images of carbon aerogels (CA) (a–c) and CA/TiO₂ (d–f) and energy dispersive X-ray spectroscopy (EDX) results for CA/TiO₂ (g).

Figure 2 presents the FTIR spectra of CA/TiO₂ and CA. The peaks at 2928 cm⁻¹ and 1096 cm⁻¹ are attributed to the C-H and C-O stretching vibrations, respectively. Compared with CA, CA/TiO₂ displayed a predominant band at 3441 cm⁻¹, which was assigned to the stretching vibration of surface water and hydroxyl groups on TiO₂ [40,41]. It is worth noting that the hydroxyl groups could reduce the recombination possibilities of photo-carriers and generate active oxygen species during the photo-catalytic process [5,40]. Moreover, the new band for CA/TiO₂ at 578 cm⁻¹ was ascribed to the vibration of Ti-O-Ti, which consistently suggested that TiO₂ had been incorporated in the carbon aerogel.

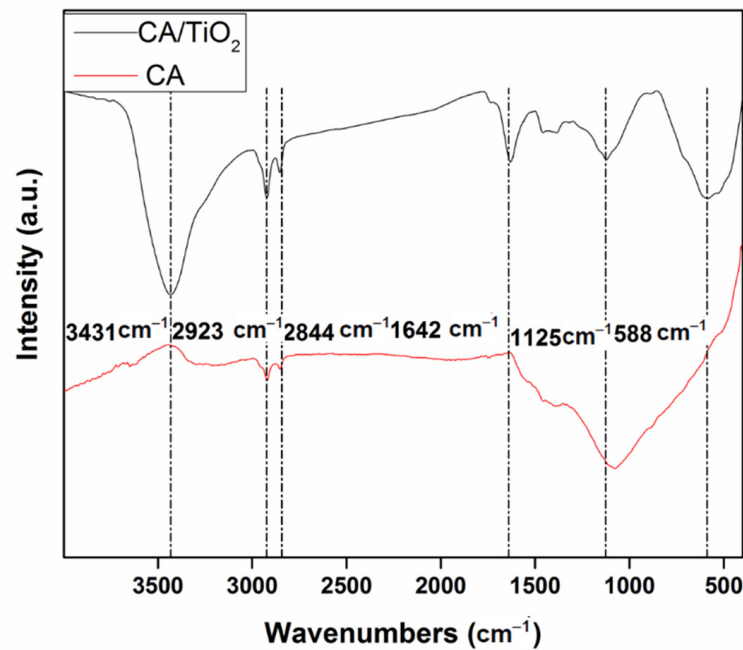


Figure 2. FTIR spectra of CA and CA/TiO₂.

A Raman spectrum was used to reveal the crystallographic characteristics of CA/TiO₂. As shown in Figure 3, the peaks at 1584 and 1336 cm⁻¹ were assigned to the D and G bands, respectively. The D band represents the sp² units adjacent to structural defects, while the G band corresponds to sp² planar and conjugated structures [42]. Furthermore, their intensity ratio of I_G/I_D was employed to depict the order extent of carbon composites. In this study, the calculated I_G/I_D value of CA/TiO₂ was 1.02, smaller than that of CA without TiO₂, as reported previously [37]. This implied the increased defects and lattice disorders of carbon in CA/TiO₂ [43,44]. The band at 151 cm⁻¹ represented the E_g model of anatase TiO₂ [45]. Some early studies revealed that anatase TiO₂ has higher photo-catalytic activity, which would benefit the photo-catalytic efficiency of CA/TiO₂ [46].

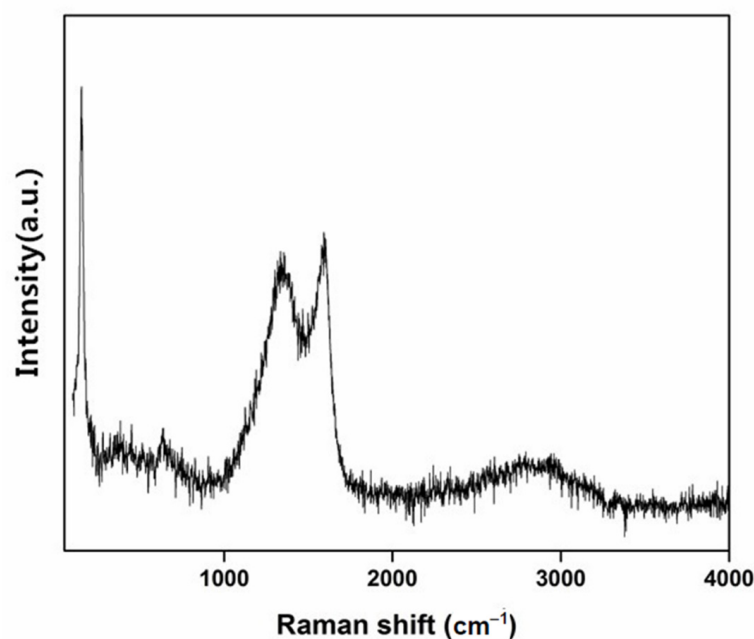


Figure 3. Raman spectrum of CA/TiO₂.

XRD was utilized to analyze the crystalline structures of CA/TiO₂. As is well known, TiO₂ has two main crystalline phases, anatase and rutile. Because of the high reactivity and chemical stability, most research interest has been focused on the anatase TiO₂ [14]. However, anatase is a metastable polymorphic form and will transform to rutile upon heating, which hardly shows any photo-catalytic activity. For pure TiO₂, this transformation roughly occurs at 730 °C, while this transition temperature varies according to the specific surface area, the particle size of TiO₂, and its purity [47,48]. Furthermore, the presence of carbon phase could also affect the crystal growth of TiO₂ in the corresponding composite [49,50]. Figure 4 depicts the XRD pattern of CA/TiO₂. The strong peaks at $2\theta = 25.5^\circ, 35.3^\circ, 38.0^\circ, 41.1^\circ, 54.1^\circ, 55.1^\circ,$ and 62.5° could be indexed to the (101), (004), (200), (105), (211), (204), and (215) crystal planes of anatase, respectively. It is interesting to notice that only anatase was observed in the XRD pattern. This seems contradictory to previous reports that when samples were carbonized at 800 °C, only rutile existed in the final products. It was believed that the interaction between the carbon phase and the anatase phase could have avoided the agglomeration and sintering of TiO₂ particles and effectively stabilized the anatase phase, preventing the transformation from anatase to rutile, even at a high temperature [35].

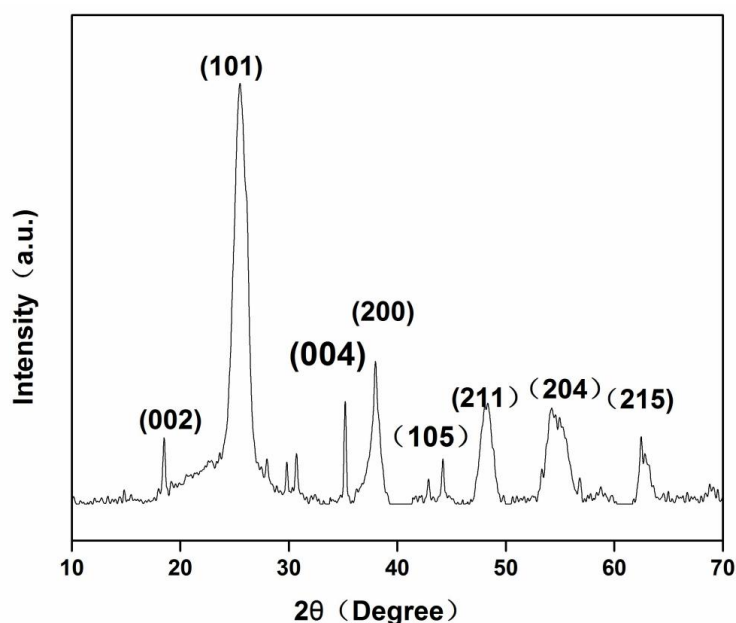


Figure 4. XRD pattern of CA/TiO₂.

XPS (Figure 5a) was used to analyze the surface chemical composition of CA/TiO₂. According to the literature, pure TiO₂ presents only one peak of Ti⁴⁺, located at the binding energy BE = 459.1 eV in a deconvoluted Ti_{2p} spectrum [51]. However, the deconvoluted Ti_{2p} spectrum of CA/TiO₂ (Figure 5b) displayed two components at 459.1 and 458.0 eV, respectively. The first peak corresponded to the Ti⁴⁺, while the other peak at 458.0 eV was attributed to the Ti³⁺ [52], suggesting that there was a reduction reaction of organic phase during carbonization [35,52].

In the XPS spectrum of O1s (Figure 5c), four peaks located at BE = 529.9, 531.6, 532.9, and 533.8 eV could be observed. As previously reported, the component at BE = 530.2 eV was assigned to the oxygen bonded to Ti⁴⁺, and the peak at BE = 531.3 eV corresponded to the oxygen bonded to Ti³⁺ [48]. The two components at 532.9 and 533.6 eV were attributed to the oxygenated surface groups of the carbon phase, like C=O and C-O. Notably, these oxygen-containing groups not only favored the dispersing and anchoring of TiO₂ on the carbon scaffold, but also substituted for the lattice oxygen and formed Ti-O-C bonds, giving rise to carbon doping [53–56].

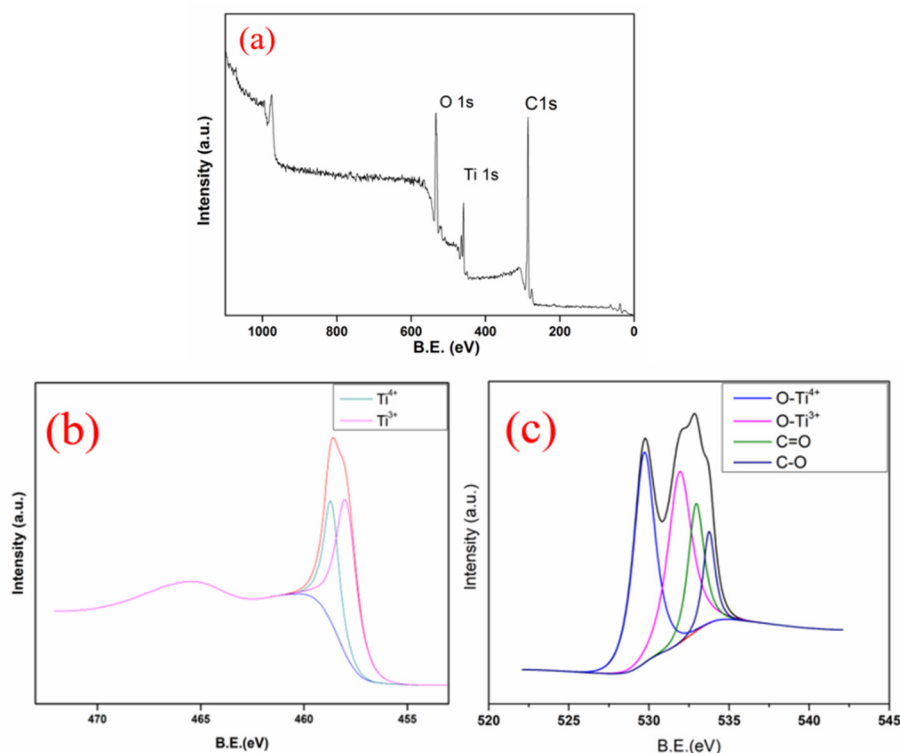


Figure 5. XPS spectrum (a) and deconvoluted Ti_{2p} spectrum (b) and O1s spectrum (c) of CA/TiO₂.

3.2. Optical Property

Due to the intrinsic band gap, TiO₂ could only absorb ultraviolet light. Figure 6 shows the diffuse reflectance UV–vis spectrum of CA/TiO₂, which displayed a strong absorption in the visible light wavelength range of 400–800 nm. This result can be attributed to the following reasons. On the one hand, the quantum confinement by the well-dispersed TiO₂ on the carbon scaffold and the carbon-doping as a result of the formation of Ti–O–C could remarkably narrow the band gap of TiO₂ [54,57]. On the other hand, the oxygen vacancies generated during carbonization and the partially reduced Ti⁴⁺ as confirmed by XPS might have acted as a new state in between the band gap of TiO₂, leading to the intense visible light absorption. This agrees well with a recent study on CNT/TiO₂ for water splitting [58].

3.3. Adsorption and Photo-Catalytic Activity Study

Figure 7 displays the MB adsorption curve of CA/TiO₂. The adsorption capacity of CA/TiO₂ for MB increased with the increase of MB concentration in the solution. Additionally, the maximum adsorption capacity was 18.5 mg/g, higher than those of many other similar materials. For example, Zhang [59] et al. prepared a TiO₂/carbon@TiO₂ composite with a core–shell structure; its adsorption capacity was 11.4 mg/g. Wang [54] prepared a TiO₂/carbon composite using cotton as the carbon source, which exhibited an adsorption capacity of 8 mg/g.

The improved adsorption capacity of CA/TiO₂ should be ascribed to the large amount of hydroxyl groups presented in CA/TiO₂, which had a preferable affinity with the positively charged MB molecule. Additionally, the abundant interconnected pores favored the diffusing process of MB from the solution into the material. As a consequence, more MB molecules could be attracted around TiO₂, giving rise to improved photo-catalytic efficiency.

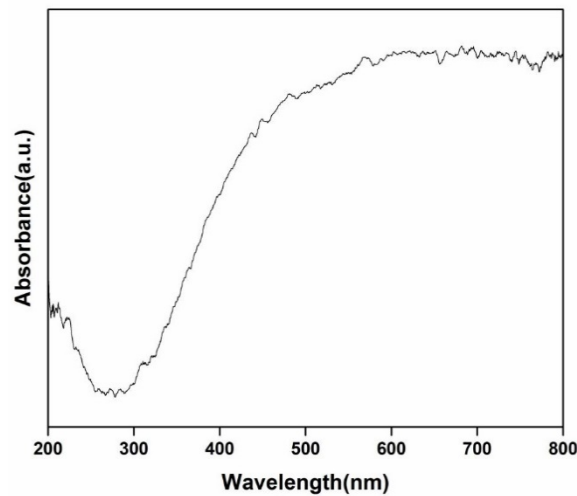


Figure 6. Diffuse reflectance spectrum of CA/TiO₂.

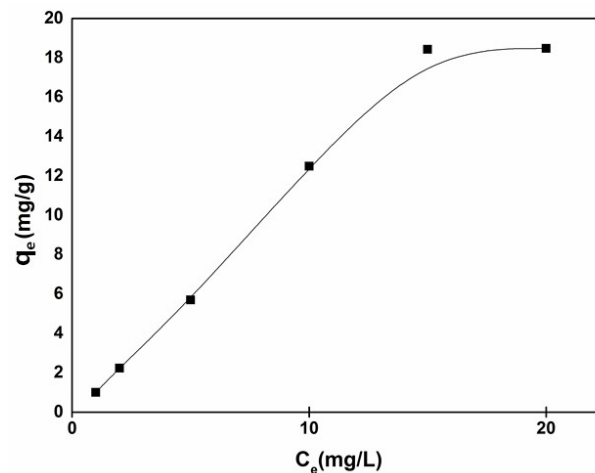


Figure 7. Adsorption isotherm of methylene blue (MB).

The photo-catalytic activity of CA/TiO₂ was evaluated by monitoring the degradation of MB under a common incandescent lamp. Because the aerogel materials also had a strong adsorption towards MB, all samples were saturated with MB under dark conditions prior to the testing of photo-catalytic activity. Figure 8 compares the photo-catalytic performance of CA/TiO₂ and CA. As expected, CA exhibited no photo-catalytic activity. By contrast, CA/TiO₂ could efficiently degrade MB. Using only 15 mg of CA/TiO₂, nearly 85% of MB in 50 mL solution with a concentration of 10 mg/L was degraded in 300 min, and the initial solution in blue was almost completely decolorized after photo-degradation (see the inset image in Figure 8). In addition, the first-order degradation kinetics plot of MB by CA/TiO₂ was analyzed and is shown in Figure 9 [54]. The plot appeared to have good linearity with a high correlation coefficient ($R^2 = 0.9828$) and a k value of 0.0039 min^{-1} . It is noteworthy that the photo-catalytic efficiency of CA/TiO₂ was higher than those of many other similar photo-catalysts in the literature. For example, Esther [35] et al. prepared a carbon xerogel–TiO₂ composite, and 800 mg of the photo-catalyst removed 90% of dye (800 mL, 10 mg/L) in 400 min. Wang [54] et al. used a TiO₂–carbon fiber composite as the photo-catalyst to degrade MB under visible light. The results indicated that 120 mg composite could degrade 80% of the dye in 100 mL MB solution (10 mg/L) after 10 h. Chen [60] et al. synthesized a TiO₂/carbon photo-catalyst to degrade MB under visible light, and 125 mg of the photo-catalyst degraded 90% MB in 250 mL solution (5 mg/L) after 7 h.

The superior photo-catalytic activity of CA/TiO₂ could be explained by the following facts. The catalytic active site of TiO₂ was anchored on the surface of carbon fiber to form a thin layer. This structure could reduce the distance that the photo-generated electrons and holes need to travel and decrease the recombination probability between these electrons and holes. Additionally, CA/TiO₂ had a highly porous and interconnected three-dimensional framework structure, which could effectively prohibit the generation of boundaries and defects (which often lead to the recombination of photo-generated electron-hole pairs) due to carbon aggregation. Last but not least, the high adsorption capacity of CA/TiO₂ resulted in the enrichment of MB around TiO₂, which improved the contact between MB and the photo-catalyst and ultimately enhanced the photo-catalytic efficiency.

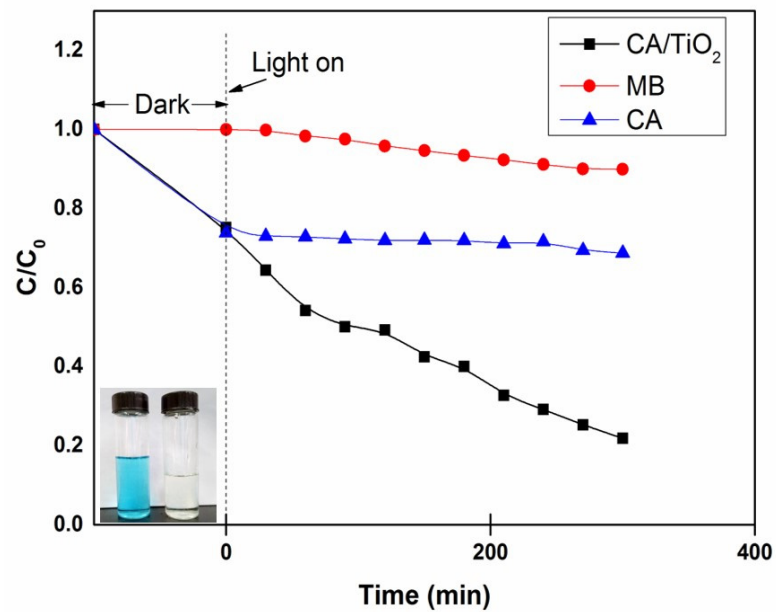


Figure 8. Photo-catalytic degradation of MB by CA/TiO₂ and CA. The insert shows the color change of the solution before and after the CA/TiO₂ treatment.

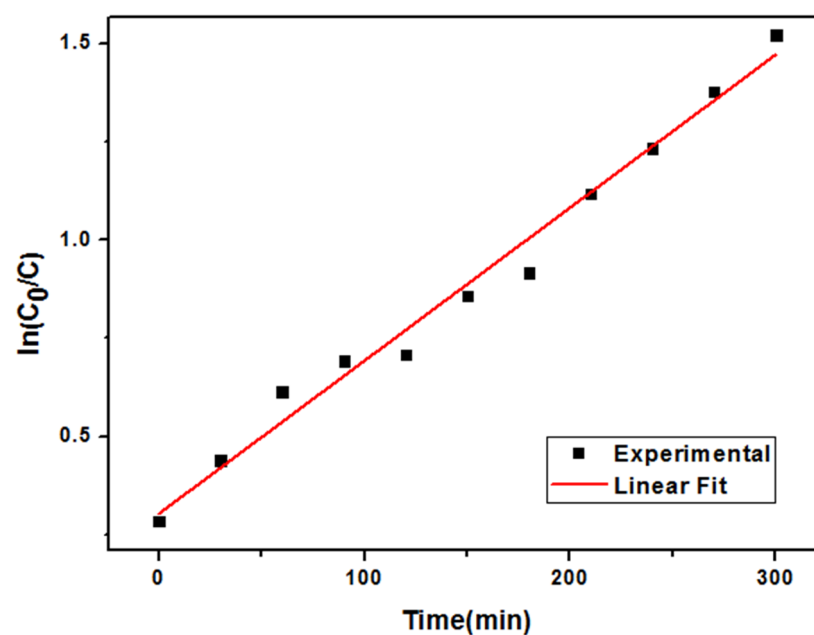


Figure 9. First-order degradation kinetics plot of MB by CA/TiO₂.

4. Conclusions

In this work, CA/TiO₂ was synthesized via hydrothermal and carbonization processes using bamboo pulp fibers and Ti(OBu)₄ as the raw materials. An instrumental analysis indicated that the catalytic active site of TiO₂ was well dispersed and homogeneously anchored on the surface of carbon fibers. The obtained TiO₂ had a crystalline structure indexed to anatase. This was resultant from the interaction between carbon and TiO₂, which prevented the transformation from anatase to rutile during the high-temperature carbonization process. The obtained CA/TiO₂ was highly porous and exhibited outstanding adsorption and photo-catalytic properties for MB decolorization. It is envisaged that the high-performance CA/TiO₂ photo-catalyst from low-cost and sustainable bioresources may find great potential in treating organic dye polluted wastewaters.

Author Contributions: Conceptualization, J.Z. (Jian Zhang) and W.Y.; data curation, Q.W.; formal analysis, J.Z. (Jian Zhang), W.Y., and C.A.; funding acquisition, W.Z. and C.L.; investigation, J.Z. (Jiangqi Zhao); methodology, J.Z. (Jian Zhang) and W.Y.; project administration, W.Z. and C.L.; resources, B.H.; software, J.Z. (Jian Zhang) and T.X.; supervision, C.L.; validation, J.Z. (Jian Zhang), W.Y., and W.Z.; visualization, J.Z. (Jian Zhang); writing—original draft, J.Z. (Jian Zhang) and W.Y.; writing—review and editing, W.Z. All authors have read and agreed to the published version of the manuscript.

Funding: This research was funded by the National Natural Science Foundation of China (51861165203), the Sichuan Science and Technology Program (2019YJ0125), the State Key Laboratory of Polymer Materials Engineering (sklpme2019-2-19), the Opening Project of Guangxi Key Laboratory of Calcium Carbonate Resources Comprehensive Utilization (HZXYKFKT201902), and the Special Foundation for Innovation-Driven Development of Hezhou (Hekechuang PT0710004).

Institutional Review Board Statement: Not applicable.

Informed Consent Statement: Not applicable.

Data Availability Statement: The data presented in this study are available within this article. Further inquiries may be directed to the authors.

Conflicts of Interest: The authors declare no conflict of interest.

References

1. Rafatullah, M.; Sulaiman, O.; Hashim, R.; Ahmad, A. Adsorption of methylene blue on low-cost adsorbents: A review. *J. Hazard. Mater.* **2010**, *177*, 70–80. [[CrossRef](#)] [[PubMed](#)]
2. Ghosh, D.; Bhattacharyya, K.G. Adsorption of methylene blue on kaolinite. *Appl. Clay Sci.* **2002**, *20*, 295–300. [[CrossRef](#)]
3. Tan, I.A.W.; Ahmad, A.L.; Hameed, B.H. Adsorption of basic dye on high-surface-area activated carbon prepared from coconut husk: Equilibrium, kinetic and thermodynamic studies. *J. Hazard. Mater.* **2008**, *154*, 337–346. [[CrossRef](#)] [[PubMed](#)]
4. Tan, I.A.W.; Ahmad, A.L.; Hameed, B.H. Adsorption of basic dye using activated carbon prepared from oil palm shell: Batch and fixed bed studies. *Desalination* **2008**, *225*, 13–28. [[CrossRef](#)]
5. Abbasi, M.; Asl, N.R. Sonochemical degradation of Basic Blue 41 dye assisted by nanoTiO₂ and H₂O₂. *J. Hazard. Mater.* **2008**, *153*, 942–947. [[CrossRef](#)] [[PubMed](#)]
6. Wu, J.-S.; Liu, C.-H.; Chu, K.H.; Suen, S.-Y. Removal of cationic dye methyl violet 2B from water by cation exchange membranes. *J. Membr. Sci.* **2008**, *309*, 239–245. [[CrossRef](#)]
7. Fan, L.; Zhou, Y.; Yang, W.; Chen, G.; Yang, F. Electrochemical degradation of aqueous solution of Amaranth azo dye on ACF under potentiostatic model. *Dye. Pigment.* **2008**, *76*, 440–446. [[CrossRef](#)]
8. Zaghbani, N.; Hafiane, A.; Dhahbi, M. Removal of Safranin T from wastewater using micellar enhanced ultrafiltration. *Desalination* **2008**, *222*, 348–356. [[CrossRef](#)]
9. Lodha, B.; Chaudhari, S. Optimization of Fenton-biological treatment scheme for the treatment of aqueous dye solutions. *J. Hazard. Mater.* **2007**, *148*, 459–466. [[CrossRef](#)]
10. Zhu, M.-X.; Lee, L.; Wang, H.-H.; Wang, Z. Removal of an anionic dye by adsorption/precipitation processes using alkaline white mud. *J. Hazard. Mater.* **2007**, *149*, 735–741. [[CrossRef](#)]
11. Lin, Y.; Li, D.; Hu, J.; Xiao, G.; Wang, J.; Li, W.; Fu, X. Highly Efficient Photocatalytic Degradation of Organic Pollutants by PANI-Modified TiO₂ Composite. *J. Phys. Chem. C* **2012**, *116*, 5764–5772. [[CrossRef](#)]
12. Huang, Y.; Ho, S.; Lu, Y.; Niu, R.; Xu, L.; Cao, J.; Lee, S. Removal of Indoor Volatile Organic Compounds via Photocatalytic Oxidation: A Short Review and Prospect. *Molecules* **2016**, *21*, 56. [[CrossRef](#)] [[PubMed](#)]

13. Herney-Ramirez, J.; Vicente, M.A.; Madeira, L.M. Heterogeneous photo-Fenton oxidation with pillared clay-based catalysts for wastewater treatment: A review. *Appl. Catal. B Environ.* **2010**, *98*, 10–26. [[CrossRef](#)]
14. Asahi, R.; Morikawa, T.; Irie, H.; Ohwaki, T. Nitrogen-Doped Titanium Dioxide as Visible-Light-Sensitive Photocatalyst: Designs, Developments, and Prospects. *Chem. Rev.* **2014**, *114*, 9824–9852. [[CrossRef](#)]
15. Asahi, R.; Morikawa, T.; Ohwaki, T.; Aoki, K.; Taga, Y. Visible-Light Photocatalysis in Nitrogen-Doped Titanium Oxides. *Science* **2001**, *293*, 269–271. [[CrossRef](#)]
16. Han, C.; Pelaez, M.; Likodimos, V.; Kontos, A.G.; Falaras, P.; O’Shea, K.; Dionysiou, D.D. Innovative visible light-activated sulfur doped TiO₂ films for water treatment. *Appl. Catal. B Environ.* **2011**, *107*, 77–87. [[CrossRef](#)]
17. Dong, F.; Guo, S.; Wang, H.; Li, X.; Wu, Z. Enhancement of the Visible Light Photocatalytic Activity of C-Doped TiO₂ Nanomaterials Prepared by a Green Synthetic Approach. *J. Phys. Chem. C* **2011**, *115*, 13285–13292. [[CrossRef](#)]
18. Su, W.; Zhang, Y.; Li, Z.; Wu, L.; Wang, X.; Li, J.; Fu, X. Multivalency Iodine Doped TiO₂: Preparation, Characterization, Theoretical Studies, and Visible-Light Photocatalysis. *Langmuir* **2008**, *24*, 3422–3428. [[CrossRef](#)]
19. Yu, J.C.; Yu, J.G.; Ho, W.; Jiang, Z.T.; Zhang, L.Z. Effects of F- Doping on the Photo-catalytic Activity and Microstructures of Nanocrystalline TiO₂ Powders. *Chem. Mater.* **2002**, *14*, 3808–3816. [[CrossRef](#)]
20. Qi, D.; Xing, M.; Zhang, J. Hydrophobic Carbon-Doped TiO₂/MCF-F Composite as a High Performance Photocatalyst. *J. Phys. Chem. C* **2014**, *118*, 7329–7336. [[CrossRef](#)]
21. Huang, J.F.; Liu, J.M.; Xiao, L.M. Facile synthesis of porous hybrid materials based on Calix-3 dye and TiO₂ for high photocatalytic water splitting performance with excellent stability. *J. Mater. Chem. A* **2019**, *7*, 2993–2999. [[CrossRef](#)]
22. Jiang, Z.; Zhu, C.; Wan, W.; Qian, K.; Xie, J. Constructing graphite-like carbon nitride modified hierarchical yolk-shell TiO₂ spheres for water pollution treatment and hydrogen production. *J. Mater. Chem. A* **2016**, *4*, 1806–1818. [[CrossRef](#)]
23. Zhang, Y.; Tang, Z.-R.; Fu, X.; Xu, Y.-J. Engineering the Unique 2D Mat of Graphene to Achieve Graphene-TiO₂ Nanocomposite for Photocatalytic Selective Transformation: What Advantage does Graphene Have over Its Forebear Carbon Nanotube? *ACS Nano* **2011**, *5*, 7426–7435. [[CrossRef](#)] [[PubMed](#)]
24. Cho, K.M.; Kim, K.H.; Choi, H.O.; Jung, H.-T. A highly photoactive, visible-light-driven graphene/2D mesoporous TiO₂ photocatalyst. *Green Chem.* **2015**, *17*, 3972–3978. [[CrossRef](#)]
25. Xing, M.; Li, X.; Zhang, J. Synergistic effect on the visible light activity of Ti³⁺ doped TiO₂ nanorods/boron doped graphene composite. *Sci. Rep.* **2014**, *4*, 5493. [[CrossRef](#)] [[PubMed](#)]
26. Tan, L.-L.; Ong, W.-J.; Chai, S.-P.; Mohamed, A.R. Reduced graphene oxide-TiO₂ nanocomposite as a promising visible-light-active photocatalyst for the conversion of carbon dioxide. *Nanoscale Res. Lett.* **2013**, *8*, 465. [[CrossRef](#)]
27. Cai, X.; Li, J.; Liu, Y. Titanium dioxide-coated biochar composites as adsorptive and photocatalytic degradation materials for the removal of aqueous organic pollutants. *Chem. Technol. Biotechnol.* **2018**, *93*, 783–791. [[CrossRef](#)]
28. Lee, W.J.; Lee, J.M.; Kochuveedu, S.T.; Han, T.H.; Jeong, H.Y.; Park, M.; Yun, J.M.; Kwon, J.; No, K.; Kim, D.H.; et al. Biom mineralized N-Doped CNT/TiO₂ Core/Shell Nanowires for Visible Light Photocatalysis. *ACS Nano* **2012**, *6*, 935–943. [[CrossRef](#)]
29. Reddy, K.R.; Hassan, M.; Gomes, V.G. Hybrid nanostructures based on titanium dioxide for enhanced photocatalysis. *Appl. Catal. A Gen.* **2015**, *489*, 1–16. [[CrossRef](#)]
30. Zhao, L.; Chen, X.; Wang, X.; Zhang, Y.; Wei, W.; Sun, Y.; Antonietti, M.; Titirici, M.M. One-Step Solvothermal Synthesis of a Carbon@TiO₂ Dyad Structure Effectively Promoting Visible-Light Photocatalysis. *Adv. Mater.* **2010**, *22*, 3317–3321. [[CrossRef](#)]
31. Zhuang, J.; Tian, Q.; Zhou, H.; Liu, Q.; Liu, P.; Zhong, H. Hierarchical porous TiO₂@C hollow microspheres: One-pot synthesis and enhanced visible-light photocatalysis. *J. Mater. Chem.* **2012**, *22*, 7036–7042. [[CrossRef](#)]
32. Zhao, D.; Sheng, G.; Chen, C.; Wang, X. Enhanced photocatalytic degradation of methylene blue under visible irradiation on graphene@TiO₂ dyad structure. *Appl. Catal. B Environ.* **2012**, *111–112*, 303–308. [[CrossRef](#)]
33. Tan, L.-L.; Ong, W.-J.; Chai, S.-P.; Goh, B.T.; Mohamed, A.R. Visible-light-active oxygen-rich TiO₂ decorated 2D graphene oxide with enhanced photocatalytic activity toward carbon dioxide reduction. *Appl. Catal. B Environ.* **2015**, *179*, 160–170. [[CrossRef](#)]
34. Li, X.; Jiang, Y.; Cheng, W.; Li, Y.; Xu, X.; Lin, K. Mesoporous TiO₂/Carbon Beads: One-Pot Preparation and Their Application in Visible-Light-Induced Photodegradation. *Nano-Micro Lett.* **2015**, *7*, 243–254. [[CrossRef](#)] [[PubMed](#)]
35. Bailón-García, E.; Elmouwahidi, A.; Álvarez, M.A.; Carrasco-Marín, F.; Pérez-Cadenas, A.F.; Maldonado-Hódar, F.J. New carbon xerogel-TiO₂ composites with high performance as visible-light photocatalysts for dye mineralization. *Appl. Catal. B Environ.* **2017**, *201*, 29–40. [[CrossRef](#)]
36. Moreno-Castilla, C.; Maldonado-Hódar, F.J. Carbon aerogels for catalysis applications: An overview. *Carbon* **2005**, *43*, 455–465. [[CrossRef](#)]
37. Yuan, W.; Zhang, X.; Zhao, J.; Li, Q.; Ao, C.; Xia, T.; Zhang, W.; Lu, C. Ultra-lightweight and highly porous carbon aerogels from bamboo pulp fibers as an effective sorbent for water treatment. *Results Phys.* **2017**, *7*, 2919–2924. [[CrossRef](#)]
38. Li, Y.-Q.; Samad, Y.A.; Polychronopoulou, K.; Alhassan, S.M.; Liao, K. Carbon Aerogel from Winter Melon for Highly Efficient and Recyclable Oils and Organic Solvents Absorption. *ACS Sustain. Chem. Eng.* **2014**, *2*, 1492–1497. [[CrossRef](#)]
39. Han, S.; Sun, Q.; Zheng, H.; Li, J.; Jin, C. Green and facile fabrication of carbon aerogels from cellulose-based waste newspaper for solving organic pollution. *Carbohydr. Polym.* **2016**, *136*, 95–100. [[CrossRef](#)]
40. He, D.; Li, Y.; Wang, L.; Wu, J.; Yang, Y.; An, Q. Carbon wrapped and doped TiO₂ mesoporous nanostructure with efficient visible-light photocatalysis for NO removal. *Appl. Surf. Sci.* **2017**, *391*, 318–325. [[CrossRef](#)]
41. Kataoka, S.; Tejedor-Tejedor, M.I.; Coronado, J.M.; Anderson, M.A. Thin-film transmission IR spectroscopy as an in situ probe of the gas–solid interface in photocatalytic processes. *J. Photochem. Photobiol. A Chem.* **2004**, *163*, 323–329. [[CrossRef](#)]

42. Sang, Y.; Zhao, Z.; Tian, J.; Hao, P.; Jiang, H.; Liu, H.; Claverie, J.P. Enhanced Photocatalytic Property of Reduced Graphene Oxide/TiO₂ Nanobelt Surface Heterostructures Constructed by an In Situ Photochemical Reduction Method. *Small* **2014**, *10*, 3775–3782. [[CrossRef](#)] [[PubMed](#)]
43. Yu, X.; Liu, J.; Yu, Y.; Zuo, S.; Li, B. Preparation and visible light photocatalytic activity of carbon quantum dots/TiO₂ nanosheet composites. *Carbon* **2014**, *68*, 718–724. [[CrossRef](#)]
44. Guo, S.; Zhang, G.; Guo, Y.; Yu, J.C. Graphene oxide-Fe₂O₃ hybrid material as highly efficient heterogeneous catalyst for degradation of organic contaminants. *Carbon* **2013**, *60*, 437–444. [[CrossRef](#)]
45. Marie, J.; Berthon-Fabry, S.; Chatenet, M.; Chainet, E.; Pirard, R.; Cornet, N.; Achard, P. Platinum supported on resorcinol-formaldehyde based carbon aerogels for PEMFC electrodes: Influence of the carbon support on electrocatalytic properties. *J. Appl. Electrochem.* **2007**, *37*, 147–153. [[CrossRef](#)]
46. Wiener, M.; Reichenauer, G.; Braxmeier, S.; Hemberger, F.; Ebert, H.-P. Carbon Aerogel-Based High-Temperature Thermal Insulation. *Int. J. Thermophys.* **2009**, *30*, 1372–1385. [[CrossRef](#)]
47. Bock, V.; Nilsson, O.; Blumm, J.; Fricke, J. Thermal properties of carbon aerogels. *J. Non-Cryst. Solids* **1995**, *185*, 233–239. [[CrossRef](#)]
48. Hanaor, D.A.H.; Sorrell, C.C. Review of the anatase to rutile phase transformation. *J. Mater. Sci.* **2011**, *46*, 855–874. [[CrossRef](#)]
49. Maldonado-Hódar, F.J.; Moreno-Castilla, C.; Rivera-Utrilla, J. Synthesis, pore texture and surface acid–base character of TiO₂/carbon composite xerogels and aerogels and their carbonized derivatives. *Appl. Catal. A Gen.* **2000**, *203*, 151–159. [[CrossRef](#)]
50. Moreno-Castilla, C.; Maldonado-Hodar, F.J. Synthesis and surface characteristics of silica- and alumina-carbon composite xerogels. *Phys. Chem. Chem. Phys.* **2000**, *2*, 4818–4822. [[CrossRef](#)]
51. Gonzalez-Elipe, A.R.; Malet, P.; Espinos, J.P.; Caballero, A.; Munuera, G. Effect of Water in the Encapsulation of the Metallic Phase During Smsi Generation in Pt/TiO₂ Catalysts. *Struct. React. Surf.* **1989**, *48*, 427–436. [[CrossRef](#)]
52. González-Elipe, A.R.; Fernández, A.; Espinós, J.P.; Munuera, G. Role of hydrogen in the mobility of phases in Ni TiOx systems. *J. Catal.* **1991**, *131*, 51–59. [[CrossRef](#)]
53. Pastrana-Martínez, L.M.; Morales-Torres, S.; Likodimos, V.; Falaras, P.; Figueiredo, J.L.; Faria, J.L.; Silva, A.M.T. Role of oxygen functionalities on the synthesis of photocatalytically active graphene–TiO₂ composites. *Appl. Catal. B Environ.* **2014**, *158–159*, 329–340. [[CrossRef](#)]
54. Wang, B.; Karthikeyan, R.; Lu, X.-Y.; Xuan, J.; Leung, M.K.H. High photocatalytic activity of immobilized TiO₂ nanorods on carbonized cotton fibers. *J. Hazard. Mater.* **2013**, *263*, 659–669. [[CrossRef](#)] [[PubMed](#)]
55. Wang, H.; Wu, Z.; Liu, Y. A Simple Two-Step Template Approach for Preparing Carbon-Doped Mesoporous TiO₂ Hollow Microspheres. *J. Phys. Chem. C* **2009**, *113*, 13317–13324. [[CrossRef](#)]
56. Zhang, Y.; Zhao, Z.; Chen, J.; Cheng, L.; Chang, J.; Sheng, W.; Hu, C.; Cao, S. C-doped hollow TiO₂ spheres: In situ synthesis, controlled shell thickness, and superior visible-light photocatalytic activity. *Appl. Catal. B Environ.* **2015**, *165*, 715–722. [[CrossRef](#)]
57. Monticone, S.; Tufeu, R.; Kanaev, A.V.; Scolan, E.; Sanchez, C. Quantum size effect in TiO₂ nanoparticles: Does it exist? *Appl. Surf. Sci.* **2000**, *162–163*, 565–570. [[CrossRef](#)]
58. Moya, A.; Cherevan, A.; Marchesan, S.; Gebhardt, P.; Prato, M.; Eder, D.; Vilatela, J.J. Oxygen vacancies and interfaces enhancing photocatalytic hydrogen production in mesoporous CNT/TiO₂ hybrids. *Appl. Catal. B Environ.* **2015**, *179*, 574–582. [[CrossRef](#)]
59. Zhang, G.; Teng, F.; Zhao, C.; Chen, L.; Zhang, P.; Wang, Y.; Gong, C.; Zhang, Z.; Xie, E. Enhanced photocatalytic activity of TiO₂/carbon@TiO₂ core–shell nanocomposite prepared by two-step hydrothermal method. *Appl. Surf. Sci.* **2014**, *311*, 384–390. [[CrossRef](#)]
60. Chen, D.; Jiang, Z.; Geng, J.; Wang, A.Q.; Yang, D. Carbon and Nitrogen Co-doped TiO₂ with Enhanced Visible-Light Photocatalytic Activity. *Huazhong Norm. Univ. J. Postgrad.* **2010**, *46*, 2741–2746. [[CrossRef](#)]